Multipartite Entangled States in Dipolar Quantum Simulators

Tommaso Comparin, Fabio Mezzacapo, and Tommaso Roscilde
Université de Lyon, Ens de Lyon, CNRS, Laboratoire de Physique, F-69342 Lyon, France

(Received 24 May 2022; accepted 14 September 2022; published 7 October 2022)

The scalable production of multipartite entangled states in ensembles of qubits is a crucial function of quantum devices, as such states are an essential resource both for fundamental studies on entanglement, as well as for applied tasks. Here we focus on the U(1) symmetric Hamiltonians for qubits with dipolar interactions—a model realized in several state-of-the-art quantum simulation platforms for lattice spin models, including Rydberg-atom arrays with resonant interactions. Making use of exact and variational simulations, we theoretically show that the nonequilibrium dynamics generated by this Hamiltonian shares fundamental features with that of the one-axis-twisting model, namely, the simplest interacting collective-spin model with U(1) symmetry. The evolution governed by the dipolar Hamiltonian generates a cascade of multipartite entangled states—spin-squeezed states, Schrödinger's cat states, and multicomponent superpositions of coherent spin states. Investigating systems with up to $N = 144$ qubits, we observe full scalability of the entanglement features of these states directly related to metrology, namely, scalable spin squeezing at an evolution time $\mathcal{O}(N^{1/3})$ and Heisenberg scaling of sensitivity of the spin parity to global rotations for cat states reached at times $\mathcal{O}(N)$. Our results suggest that the native Hamiltonian dynamics of state-of-the-art quantum simulation platforms, such as Rydberg-atom arrays, can act as a robust source of multipartite entanglement.

DOI: 10.1103/PhysRevLett.129.150503

Introduction.—Quantum entanglement [1] is the distinctive feature of many-body quantum mechanics, at the root of its fundamental complexity and its potential as a technological resource [2–4]. Generic pure states in the Hilbert space have a large bipartite entanglement, captured by entanglement entropies of a subsystem that scale like the subsystem volume [5]; a similar scaling is observed in states that are obtained, e.g., by evolving initially nonentangled states with a generic interacting many-body Hamiltonian for a macroscopic time, leading to quantum thermalization [6]. Nonetheless, a more specialized form of entanglement is widely recognized as a resource, namely, "certifiable multipartite" entanglement, in which (1) the number of inseparable degrees of freedom (also known as entanglement depth [7]) is as big as a macroscopic fraction of the system, and (2) such a depth can be efficiently estimated with criteria based on the measurement of a few observables. States of this kind allow for an efficient (i.e., scalable) entanglement certification [8], and they represent the basis of quantum technology tasks, such as entanglement-assisted metrology [3,4]. Therefore, identifying robust protocols that lead to an *efficient* and *scalable* production of certifiable multipartite states—namely, of states with an entanglement depth scaling polynomially with the number N of degrees of freedom and in a time scaling polynomially with N—is a central task of modern quantum science and technology. In this Letter, we show that scalable production of multipartite entangled states can be achieved in qubit ensembles with U(1) symmetric *dipolar* interactions, which are most prominently realized by Rydberg atoms with resonant interactions [9], among other platforms [10–12]. Making use of state-of-the-art time-dependent variational approaches, pushed to macroscopic evolution times, we show that two-dimensional lattices of qubits interacting with dipolar couplings for two spin components, initialized in a coherent spin state along an interaction axis, evade generic thermalization; and they develop paradigmatic examples of multipartite entangled states, namely, spin-squeezed states [13,14] and Schrödinger's cat states [15,16]. The dynamics of dipolar systems is found to exhibit a deep similarity to that of the paradigmatic model of collective-spin interactions, namely, the one-axis-twisting (OAT) Hamiltonian [13]. In particular, we observe catlike states in dipolar lattices for up to $N = 144$ qubits—a remarkable observation in a system with non-mean-field interactions. Our Letter paves the way for the scalable production of multipartite entanglement in dipolar quantum simulators.

Certifiable multipartite entanglement.—We specialize our attention to the case of qubit ensembles, whose most basic description is achieved in terms of the collective-spin operator $\boldsymbol{J} = \sum_{i=1}^{N} \boldsymbol{S}_i$, where $\boldsymbol{S}_i$'s represent spin-1/2 operators for each of the N qubits. A primary example of certifiable multipartite entanglement in qubit ensembles is offered by spin-squeezed states [13,14], namely, entangled states that are characterized by a finite net spin orientation $\langle \boldsymbol{J} \rangle$; and by relative fluctuations of one collective-spin component transverse to the average orientation that are

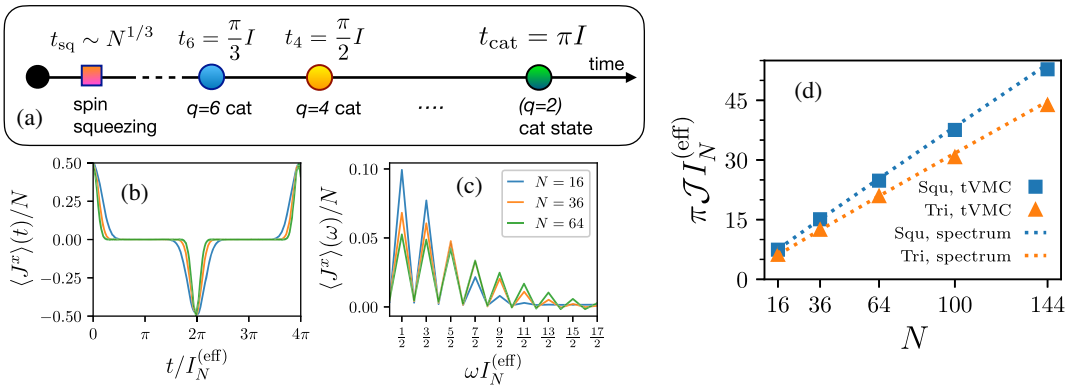

FIG. 1. (a) Cascade of entangled states observed in the OAT model and in this Letter—here we only indicate even-headed cat states, but q-headed states with odd q exist as well, at times $t = 2\pi I/q$. (b) Dynamics of the average spin $\langle J^x \rangle(t)$ for the dipolar XX model on the square lattice. (c) Fourier transform $\langle J^x \rangle(\omega)$, for coherence with the y-axis label in the figure. (d) Effective moment of inertia for the square (Squ) and triangular (Tri) dipolar lattices as extracted from the TVMC dynamics (squares and triangles) and estimated from the low-energy spectrum (dashed lines). The specific combination $\pi I_N^{(\mathrm{eff})} \mathcal{J}$ represents the time of the $q = 2$ cat state.

reduced with respect to all fully separable states. The relative fluctuations are captured by the spin-squeezing parameter [14]

$$\xi_R^2 = \frac{N \min_\perp \mathrm{Var}(J^\perp)}{|\langle \boldsymbol{J} \rangle|^2}, \tag{1}$$

where the minimization is made over the plane perpendicular to $\langle \boldsymbol{J} \rangle$, and spin squeezing amounts to the condition $\xi_R^2 < 1$. Spin squeezing is an entanglement witness [17] and it is an entanglement-depth estimator: $\xi_R^2 < 1/k$ with $k > 1$ guarantees that a state is not k-producible, namely, the smallest block of entangled qubits is composed of $k+1$ elements [18–20]. Moreover, when subject to rotations $e^{-i\theta J'_\perp}$ around the antisqueezed direction $J'_\perp$ (perpendicular to both $\langle \boldsymbol{J} \rangle$ and to the squeezed component), spin-squeezed states allow for an estimate of the angle of rotation with an uncertainty $\delta\theta = \xi_R/\sqrt{N}$ below the so-called standard quantum limit $(\delta\theta)_{\mathrm{SQL}} = 1/\sqrt{N}$. A second example of certifiable multipartite entanglement is offered by Schrödinger's cat [or Greenberger-Horne-Zeilinger (GHZ) [21]] states. Introducing the coherent spin state (CSS) with all spins polarized along the $\boldsymbol{n}$ direction, $|\mathrm{CSS}_{\boldsymbol{n}}\rangle = |\boldsymbol{n}\rangle^{\otimes N}$—with $|\pm \boldsymbol{n}\rangle$ a generic qubit state with Bloch vector $\pm\boldsymbol{n}$—the most general form for a cat state (up to local unitaries) is $|\mathrm{GHZ}_{\boldsymbol{n}}\rangle = (|\mathrm{CSS}_{\boldsymbol{n}}\rangle + e^{i\phi}|\mathrm{CSS}_{-\boldsymbol{n}}\rangle)/\sqrt{2}$. This state has an entanglement depth of N and, when rotated around the $\boldsymbol{n}$ direction with the unitary $e^{-i\theta \boldsymbol{J}\cdot\boldsymbol{n}}$, it allows for an estimate of the rotation angle with uncertainty $\delta\theta = 1/N$, representing the ultimate (Heisenberg) limit for phase estimation. A generalization of the cat state is offered by so-called q-headed cat states [15], which are superpositions of q CSSs along directions $\boldsymbol{n}_p$ $(p = 0, \ldots, q-1)$ in, e.g., the xy plane, forming an angle of $2\pi p/q$ with the x axis: $|q\,\mathrm{cat}\rangle = \mathcal{A}^{-1} \sum_{p=0}^{q-1} c_p |\mathrm{CSS}_{\boldsymbol{n}_p}\rangle$ with complex c_p coefficients of unit modulus and $\mathcal{A}$ as a normalization factor.

Long-range interacting XX Hamiltonians and OAT model.—In this Letter, we show how spin-squeezed states and catlike states are generated along the unitary dynamics initialized in the coherent spin state $|\mathrm{CSS}_x\rangle$ with $\boldsymbol{n} = \boldsymbol{e}_x$; and governed by the long-range XX ferromagnetic Hamiltonian

$$\mathcal{H}_{\alpha-XX} = -\frac{\mathcal{J}}{\mathcal{N}_\alpha} \sum_{i<j} \frac{1}{r_{ij}^\alpha} (S_i^x S_j^x + S_i^y S_j^y), \tag{2}$$

where $\mathcal{J} > 0$ is the coupling constant, r_{ij} is the distance between the ith and jth spins, and $\mathcal{N}_\alpha$ is a normalization factor ensuring an extensive energy. Throughout this Letter, we shall consider spins arranged on a planar lattice with $N = L \times L$ sites and periodic boundary conditions; we shall present results for both the square and the triangular lattice. All of our results are for dipolar ($\alpha = 3$) interactions (for which we can take $\mathcal{N}_3 = 1$), so as to realize with Eq. (2) the Hamiltonian of resonantly interacting Rydberg atoms [9]. Recent experiments [9,22–24] use pairs of Rydberg states of Rb atoms with principal quantum number $n \gtrsim 60$ to encode qubits. For these states, the coupling constant $\mathcal{J}$ can be either positive or negative depending on the chosen states—the sign being irrelevant for the dynamics initialized in the CSS_x state [25], so that we shall choose $\mathcal{J} > 0$ in what follows. For the typical interatomic spacings used in the experiment, one has that $\mathcal{J} \sim 2\pi \times 1 - 10$ MHz (taking $\hbar = 1$).

In order to understand the dynamics of the dipolar system, a fundamental reference is offered by the limit $\alpha = 0$. In this limit, taking $\mathcal{N}_0 = N$, one obtains $\mathcal{H}_{0-XX} = [(J^z)^2/2I] + c$, with $c = -(\mathcal{J}/2N)\boldsymbol{J}^2 + \mathcal{J}/4$ as a constant factor, since the Hamiltonian commutes with $\boldsymbol{J}^2$. The latter Hamiltonian is the OAT model [13] of a planar rotor with moment of inertia $I = N/\mathcal{J}$, whose

dynamics is exactly solvable. When the dynamics is initialized in the $|\mathrm{CSS}_x\rangle$ state, this model is known to generate a cascade of entangled states [4,13,15,16] [see Fig. 1(a) for a sketch], namely, (1) at a time $t_{\mathrm{sq}} \sim N^{1/3}$, a spin-squeezed state for $\xi_R^2 \sim N^{-2/3}$, and (2) (with N even) at times $t_q = 2\pi I/q$ a q-cat state—in particular, a GHZ state of the kind $|\mathrm{GHZ}_x\rangle = (|\mathrm{CSS}_x\rangle + i|\mathrm{CSS}_{-x}\rangle)/\sqrt{2}$ for $t_{\mathrm{GHZ}} = \pi I$. The OAT Hamiltonian can be realized with spinor Bose condensates in a single spatial mode, and spin squeezing has been observed in seminal experiments [26–28] (see also Ref. [29] for a trapped-ion realization); more recently, its implementation with superconducting circuits has allowed for the generation of (q-headed) cat states with up to $N = 20$ qubits [30]. The full OAT dynamics is also realized with large single-atom spins in Dy gases [31]. Several theoretical works have explored the effective realization of OAT dynamics in similar models [32–37], as well as the entanglement and Bell nonlocality content of the generated states [38–41]. The main result of this Letter is that the same sequence of entangled states generated by the OAT dynamics can be realized with the dipolar Hamiltonian (2) with $\alpha = 3$ for Rydberg atoms, with metrological qualities of the produced states that have the same scaling behavior as in the ideal case of the OAT dynamics. This result is far from trivial, as the OAT model is integrable (with nonthermalizing dynamics), while the dipolar Hamiltonian is expected to be chaotic (see discussion below).

Time-dependent variational dynamics.—To investigate the scalable production of entangled states along the dynamics generated by the dipolar XX model, we compute the exact dynamics up to $N = 20$ qubits [42,43], and for larger N we employ a time-dependent variational Monte Carlo (TVMC) scheme [44,45], based on the pair-product (or spin-Jastrow) wave function [46] $|\Psi(t)\rangle =: \sum_{\boldsymbol{\sigma}} \prod_{j\neq k} c_{jk}(\sigma_j, \sigma_k; t)|\boldsymbol{\sigma}\rangle$, where σ_i is the state of the ith spin on the computational basis (eigenbasis of S_i^z). The evolution of the pair coefficients c_{jk} is dictated by the time-dependent variational principle. This wave function captures *exactly* the dynamics of the OAT model [36]; as shown in the Supplemental Material [47], it remains extremely accurate in the case of $\alpha = 3$ on planar lattices when compared with exact calculations for small sizes; and it allows us to push the calculation of the dynamics to sizes $N \sim 100$ and to reach macroscopic evolution times $t\mathcal{J} \sim \mathcal{O}(N)$ thanks to its small number of variational parameters [$\mathcal{O}(N)$ with translational symmetry].

OAT-like dynamics of a planar dipolar array.—To establish a first link between the OAT dynamics and the dynamics of the dipolar XX model, we investigate the time evolution of the average collective spin, whose only component that is not identically zero is $\langle J^x\rangle(t)$. Figure 1(b) shows the time evolution of $\langle J^x\rangle$, exhibiting the characteristic pattern of the OAT dynamics, with an inversion of the collective-spin orientation at time t_{inv} followed by a revival of the original orientation at time t_{rev}. These two events occur at times $2\pi I$ and $4\pi I$ in the OAT dynamics, and therefore they allow us to define an *effective* size-dependent moment of inertia $I_N^{(\mathrm{eff})}$ for the dipolar system such that $t_{\mathrm{inv}} = 2\pi I_N^{(\mathrm{eff})}$ and $t_{\mathrm{rev}} = 4\pi I_N^{(\mathrm{eff})}$. The effective moment of inertia $I_N^{(\mathrm{eff})}$ for the dipolar square and triangular lattices is shown in Fig. 1(d), and it is found to scale linearly with N; in particular, the triangular lattice has a smaller $I_N^{(\mathrm{eff})}$ due to its higher connectivity, guaranteeing a faster dynamics. In fact, as further discussed in the Supplemental Material [47], $I_N^{(\mathrm{eff})}$ can be predicted *ab initio* by inspecting the low-energy excitation spectrum for a small system ($N = 16$) and recognizing in it the characteristic planar rotor spectrum (known as the Anderson tower of states [36,50,51]). This allows us to extract the moment of inertia $I_{N=16}^{(\mathrm{eff})}$, which can then be appropriately rescaled to an arbitrary size N by using Kac renormalization factors, in very good agreement with the moment of inertia extracted directly from the time dependence of system of size N [see Fig. 1(d)]. The Fourier transform of $\langle J^x\rangle(t)$ further reveals the nature of the low-lying energy spectrum of the system as that of a planar rotor: indeed, as J^x connects states with $J^z = M$ differing by one unit, one expects [47] to see characteristic frequencies with energies $\omega I_N^{(\mathrm{eff})} = [(M+1)^2 - M^2]/2 = M + 1/2$, which is precisely what is observed in Fig. 1(c).

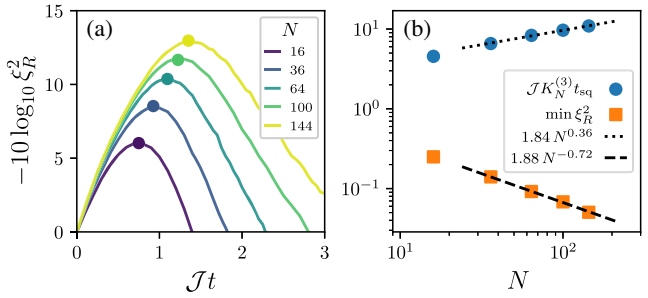

FIG. 2. (a) Evolution of the spin-squeezing parameter for the dipolar XX model on a square lattice, where the circles mark the optimum. (b) Scaling of the optimal squeezing value and optimal squeezing time (with Kac normalization $K_N^{(\alpha)}$ [47]), showing exponents $\nu = 0.72$ and $\mu = 0.36$ (to be compared with $\nu = 2/3$ and $\mu = 1/3$ for the OAT model).

Squeezed states and OAT scaling.—The first class of multipartite entangled states produced by the Hamiltonian dynamics is represented by spin-squeezed states. Figure 2 shows the time evolution for the squeezing parameter for various system sizes: scalable squeezing is exhibited, with a scaling of the optimal squeezing time and value that is compatible with the behavior of the OAT model. Our results are consistent with those of Ref. [33], based on an independent semiclassical calculation.

Multi- and double-headed cat states.—The squeezing dynamics is followed by the generation of oversqueezed states: their entanglement pattern is best recognizable at

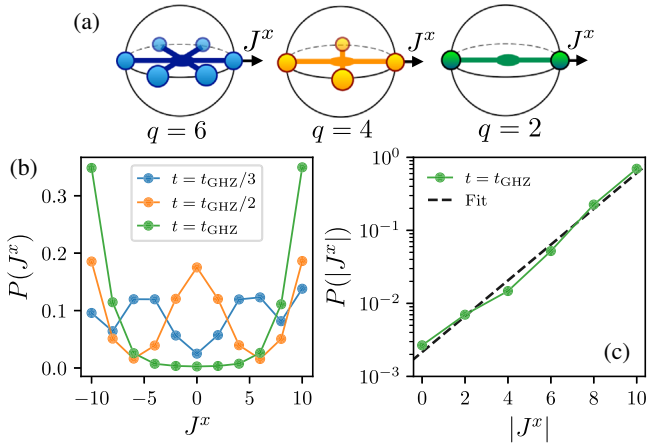

FIG. 3. (a) Sketch of the q-cat states studied here—the balls indicate the coherent states involved in the q-cat state. (b) Distributions $P(J^x)$ obtained at the times of formation of the cat states with $q = 6$, 4, and 2, obtained via exact calculations on a 5×4 square lattice—only the P values for even J^x are indicated, as the probability for the odd J^x values vanish identically, since the Hamiltonian is parity conserving. (c) Log-lin plot of the tail of the peaks for the $q = 2$ cat state; the dashed line is the fit to an exponential.

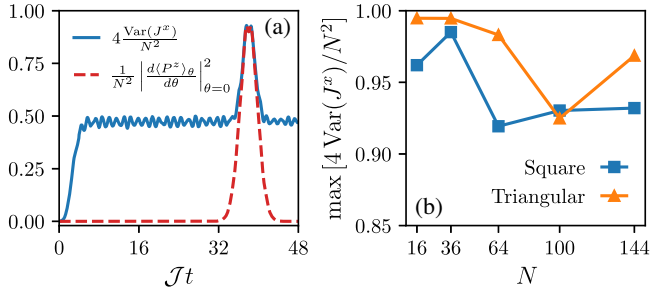

FIG. 4. (a) Time evolution of $4\mathrm{Var}(J^x)/N^2$ compared to that of the inverse uncertainty on phase estimation from the evolution of the parity—the results are for a square lattice with $N = 100$. (b) Size dependence of the maximal variance of J^x during time evolution, for both square and triangular lattices.

times $2\pi I^{(\mathrm{eff})}/q$, at which these states are expected to take the form of q-cat states [see Fig. 3(a) for a sketch]. In order to detect the appearance of a q-cat state, we inspect the probability distribution $P(J^x)$ for the J^x spin component [52], reconstructed via exact calculations in Fig. 3(b) (while in the Supplemental Material [47] we show a TVMC study of the overlap with the $|q\text{-cat}\rangle$ states). At times $2\pi I^{(\mathrm{eff})}/q$, the $P(J^x)$ distribution exhibits a multipeaked structure, reflecting the appearance of a q-cat state as superposition of several CSSs with discrete projections along the J^x axis. In particular, we observe a characteristic four-peak structure for the $q = 6$ cat state, a three-peak structure for the $q = 4$ cat state, and a two-peak structure for the $q = 2$ cat/GHZ state. In the latter case, the distribution associated with the ideal cat state would be $P(J^x) = 1/2$ for $J^x = \pm N/2$ and zero otherwise, while the dipolar cat state exhibits instead two peaks with a tail. Nonetheless, as shown in Fig. 3(c), the tail in question decays exponentially when moving away from the maxima; this localized structure of the distribution around its maxima has important consequences that we shall further explore below.

In spite of their different multipeak structures, the distributions for the $q > 2$ cat states have nearly the same variance, as shown in Fig. 4(a); therefore, their specific nature is only seen via higher moments. On the other hand, the $q = 2$ cat/GHZ state stands out for its variance $\mathrm{Var}(J^x)$, which attains the maximum possible value of $N^2/4$ for N qubits in the case of the ideal cat state; while it attains a value that approaches this maximum in the case of the state generated by the dipolar dynamics. As shown in Fig. 4(b), for the system sizes of interest the maximum of the variance $\mathrm{Var}(J^x)$ reached for dipolar cat states scales indeed with N^2, attaining a value which is $> 90\%$ of its maximum. Even though we do not have access to the $P(J^x)$ distribution within the TVMC approach, this result is fully coherent with the distribution remaining exponentially localized around $\pm N/2$ values up to the largest systems we considered.

Heisenberg-limited interferometry using parity.—The dipolar cat state of maximum variance $\mathrm{Var}(J^x)$ differs from the ideal GHZ state in that it contains pairs of macroscopically distinct states other than $|\mathrm{CSS}_{\pm x}\rangle$, as evidenced by the $P(J^x)$ distribution [Fig. 3(b)]. As a consequence, its overlap with the ideal GHZ state degrades with system size, as shown in the Supplemental Material [47]. Yet the state retains macroscopic quantum coherence, which is at the root of its extreme metrological sensitivity, representing the most significant consequence of its macroscopic entanglement depth. A fundamental figure of merit for the entanglement content of catlike states is provided by their sensitivity to rotations $U(\theta) = e^{-i\theta J^x}$, which is best captured by the θ dependence of the expectation value of the parity operator $P^z = \prod_i (2S_i^z)$, namely, $\langle P^z \rangle_\theta = \langle \Psi(t)|U(-\theta)P^z U(\theta)|\Psi(t)\rangle$. The quantum Cramér-Rao bound [4] imposes that

$$\max_{\theta^*} \frac{1}{\mathrm{Var}(P^z)_{\theta=\theta^*}} \left| \frac{d\langle P^z \rangle_\theta}{d\theta} \right|^2_{\theta=\theta^*} \leq \mathrm{QFI}(J^x) \leq 4\mathrm{Var}(J^x), \tag{3}$$

where the left-hand side expresses the inverse squared uncertainty $(\delta\theta)^{-2}$ on the angle estimation using the parity measurement, and $\mathrm{QFI}(J^x)$ is the quantum Fisher information associated with the J^x operator, which in the case of pure states coincides with the upper bound given by $4\mathrm{Var}(J^x)$. Our TVMC calculations allow us to reconstruct the left-hand side of the inequality (3) for $\theta^* = 0$ [47]. The result is shown in Fig. 4(a) and compared to $4\mathrm{Var}(J^x)$: there we see that, upon formation of the dipolar cat state, the inequality chain of Eq. (3) collapses to an identity,

showing that the measurement of the parity around $\theta^* = 0$ is optimal, as expected for cat states. This optimality is observed for all the system sizes we considered: therefore, the fact that $4\mathrm{Var}(J^x) \approx aN^2$ with $a \gtrsim 0.9$ [as shown in Fig. 4(b)] allows us to conclude that dipolar cat states can attain the Heisenberg scaling for interferometric precision and they can achieve $> 90\%$ of the Heisenberg limit.

Discussion and conclusions.—We have shown that planar qubit arrays with dipolar interactions can reproduce the entanglement dynamics of the one-axis-twisting Hamiltonian, with the scalable production of spin-squeezed states and catlike states. This result is rooted in the deep correspondence between the low-energy spectra of the two models, taking the form of a tower of states for a planar rotor. Nonetheless, the cascade of entangled states and the revivals of the initial state observed in this Letter are in clear contradiction with the picture of quantum thermalization of closed quantum systems [53], in which local observables should exhibit small fluctuations around their thermodynamic equilibrium value. This observation is at odds with the fact that the dipolar spin model is expected to be a nonintegrable one. The deviation of the observed dynamics with respect to standard thermalization can be understood within a picture in which the collective spin and the fluctuations of the spins at finite momentum effectively decouple, as we shall present in a forthcoming publication; nonetheless, this decoupling is only approximate and should break down at sufficiently long times. Yet our observation is that dipolar systems comprising $N \sim \mathcal{O}(100)$ qubits—currently accessible experimentally with Rydberg-atom arrays [54,55]—do not show any significant degradation of the decoupling picture up to macroscopic evolution times $\sim\mathcal{O}(N)$. This fundamental property of dipolar Hamiltonians implies that atomic quantum simulators realizing dipolar qubit ensembles with U(1) symmetry—Rydberg atoms [9], as well as dipolar molecules [10], trapped ions [29,56], magnetic atoms [12], etc.—have the potential to reach unprecedented levels of multipartite entanglement, including cat states with $N > 100$ and Heisenberg scaling of metrological properties. The latter scaling requires the measurement of the parity, which is perfectly accessible in state-of-the-art quantum simulators granting single-qubit addressability. In the specific case of Rydberg atoms with resonant interactions, the $\sim\mathcal{O}(N)$ evolution times required to reach large cat states may appear out of reach due to the finite lifetime of the Rydberg states; but the lifetime can be extended far beyond the requirements of our observations when using, e.g., circular Rydberg states [57].

We acknowledge useful discussions with A. Browaeys and I. Frérot. This work is supported by the Agence Nationale de la Recherche (EELS project, ANR-18-CE47-0004) and by QuantERA ("MAQS" project). All numerical simulations have been performed on the PSMN cluster of the ENS of Lyon. Exact results have been obtained through the QuSpin package [42,43]. Supporting numerical data are available in Ref. [58].

[1] R. Horodecki, P. Horodecki, M. Horodecki, and K. Horodecki, Rev. Mod. Phys. **81**, 865 (2009).
[2] J. Preskill, arXiv:1203.5813.
[3] G. Tóth and I. Apellaniz, J. Phys. A **47**, 424006 (2014).
[4] L. Pezzè, A. Smerzi, M. K. Oberthaler, R. Schmied, and P. Treutlein, Rev. Mod. Phys. **90**, 035005 (2018).
[5] D. N. Page, Phys. Rev. Lett. **71**, 1291 (1993).
[6] A. M. Kaufman, M. E. Tai, A. Lukin, M. Rispoli, R. Schittko, P. M. Preiss, and M. Greiner, Science **353**, 794 (2016).
[7] A. S. Sørensen and K. Mølmer, Phys. Rev. Lett. **86**, 4431 (2001).
[8] O. Gühne and G. Tóth, Phys. Rep. **474**, 1 (2009).
[9] A. Browaeys and T. Lahaye, Nat. Phys. **16**, 132 (2020).
[10] S. Moses, J. Covey, M. Miecnikowski, D. Jin, and J. Ye, Nat. Phys. **13**, 13 (2017).
[11] G. Kucsko, S. Choi, J. Choi, P. C. Maurer, H. Zhou, R. Landig, H. Sumiya, S. Onoda, J. Isoya, F. Jelezko *et al.*, Phys. Rev. Lett. **121**, 023601 (2018).
[12] L. Chomaz, I. Ferrier-Barbut, F. Ferlaino, B. Laburthe-Tolra, B. L. Lev, and T. Pfau, arXiv:2201.02672.
[13] M. Kitagawa and M. Ueda, Phys. Rev. A **47**, 5138 (1993).
[14] D. J. Wineland, J. J. Bollinger, W. M. Itano, and D. J. Heinzen, Phys. Rev. A **50**, 67 (1994).
[15] G. S. Agarwal, R. R. Puri, and R. P. Singh, Phys. Rev. A **56**, 2249 (1997).
[16] K. Mølmer and A. Sørensen, Phys. Rev. Lett. **82**, 1835 (1999).
[17] A. Sørensen, L.-M. Duan, J. I. Cirac, and P. Zoller, Nature (London) **409**, 63 (2001).
[18] L. Pezzé and A. Smerzi, Phys. Rev. Lett. **102**, 100401 (2009).
[19] P. Hyllus, W. Laskowski, R. Krischek, C. Schwemmer, W. Wieczorek, H. Weinfurter, L. Pezzé, and A. Smerzi, Phys. Rev. A **85**, 022321 (2012).
[20] G. Tóth, Phys. Rev. A **85**, 022322 (2012).
[21] D. M. Greenberger, M. A. Horne, and A. Zeilinger, *Going Beyond Bell's Theorem* (Springer Netherlands, Dordrecht, 1989), ISBN:978-94-017-0849-4, pp. 69–72.
[22] D. Barredo, H. Labuhn, S. Ravets, T. Lahaye, A. Browaeys, and C. S. Adams, Phys. Rev. Lett. **114**, 113002 (2015).
[23] S. de Léséleuc, V. Lienhard, P. Scholl, D. Barredo, S. Weber, N. Lang, H. P. Büchler, T. Lahaye, and A. Browaeys, Science **365**, 775 (2019).
[24] C. Chen, G. Bornet, M. Bintz, G. Emperauger, L. Leclerc, V. S. Liu, P. Scholl, D. Barredo, J. Hauschild, S. Chatterjee *et al.*, arXiv:2207.12930.
[25] I. Frérot, P. Naldesi, and T. Roscilde, Phys. Rev. Lett. **120**, 050401 (2018).
[26] J. Estève, C. Gross, A. Weller, S. Giovanazzi, and M. K. Oberthaler, Nature (London) **455**, 1216 (2008).
[27] M. F. Riedel, P. Böhi, Y. Li, T. W. Hänsch, A. Sinatra, and P. Treutlein, Nature (London) **464**, 1170 (2010).
[28] O. Hosten, N. J. Engelsen, R. Krishnakumar, and M. A. Kasevich, Nature (London) **529**, 505 (2016).

[29] J. G. Bohnet, B. C. Sawyer, J. W. Britton, M. L. Wall, A. M. Rey, M. Foss-Feig, and J. J. Bollinger, Science **352**, 1297 (2016).
[30] C. Song, K. Xu, H. Li, Y.-R. Zhang, X. Zhang, W. Liu, Q. Guo, Z. Wang, W. Ren, J. Hao *et al.*, Science **365**, 574 (2019).
[31] T. Chalopin, C. Bouazza, A. Evrard, V. Makhalov, D. Dreon, J. Dalibard, L. A. Sidorenkov, and S. Nascimbene, Nat. Commun. **9** (2018).
[32] D. Kajtoch, E. Witkowska, and A. Sinatra, Europhys. Lett. **123**, 20012 (2018).
[33] M. A. Perlin, C. Qu, and A. M. Rey, Phys. Rev. Lett. **125**, 223401 (2020).
[34] T. Bilitewski, L. De Marco, J.-R. Li, K. Matsuda, W. G. Tobias, G. Valtolina, J. Ye, and A. M. Rey, Phys. Rev. Lett. **126**, 113401 (2021).
[35] M. Płodzień, M. Kościelski, E. Witkowska, and A. Sinatra, Phys. Rev. A **102**, 013328 (2020).
[36] T. Comparin, F. Mezzacapo, and T. Roscilde, Phys. Rev. A **105**, 022625 (2022).
[37] T. H. Yanes, M. Płodzień, M. M. Sinkevičienė, G. Žlabys, G. Juzeliūnas, and E. Witkowska, Phys. Rev. Lett. **129**, 090403 (2022).
[38] R. Schmied, J.-D. Bancal, B. Allard, M. Fadel, V. Scarani, P. Treutlein, and N. Sangouard, Science **352**, 441 (2016).
[39] A. Aloy, J. Tura, F. Baccari, A. Acín, M. Lewenstein, and R. Augusiak, Phys. Rev. Lett. **123**, 100507 (2019).
[40] F. Baccari, J. Tura, M. Fadel, A. Aloy, J.-D. Bancal, N. Sangouard, M. Lewenstein, A. Acín, and R. Augusiak, Phys. Rev. A **100**, 022121 (2019).
[41] M. Płodzień, M. Lewenstein, E. Witkowska, and J. Chwedeńczuk, arXiv:2206.10542.
[42] P. Weinberg and M. Bukov, SciPost Phys. **2**, 003 (2017).
[43] P. Weinberg and M. Bukov, SciPost Phys. **7**, 20 (2019).
[44] G. Carleo, F. Becca, M. Schiró, and M. Fabrizio, Sci. Rep. **2**, 243 (2012).
[45] F. Becca and S. Sorella, *Quantum Monte Carlo Approaches for Correlated Systems* (Cambridge University Press, Cambridge, England, 2017).
[46] J. Thibaut, T. Roscilde, and F. Mezzacapo, Phys. Rev. B **100**, 155148 (2019).
[47] See Supplemental Material at http://link.aps.org/supplemental/10.1103/PhysRevLett.129.150503 for details about (1) the validation of the pair-product ansatz, (2) the calculation of the effective moment of inertia for the dipolar system, (3) the quench spectroscopy of the tower-of-states spectrum, (4) the TVMC computation of state overlaps, (5) the TVMC study of overlaps with q-cat states, (6) the fidelity between the dipolar cat states and GHZ states, and (7) the TVMC calculation of parity derivatives with respect to rotation angle, which includes Refs. [48,49].
[48] M. Medvidović and G. Carleo, npj Quantum Inf. **7** (2021).
[49] A. Omran, H. Levine, A. Keesling, G. Semeghini, T. T. Wang, S. Ebadi, H. Bernien, A. S. Zibrov, H. Pichler, S. Choi *et al.*, Science **365**, 570 (2019).
[50] P. W. Anderson, *Basic Notions of Condensed Matter Physics* (Taylor & Francis, Boca Raton, FL, 1997).
[51] H. Tasaki, J. Stat. Phys. **174**, 735 (2019).
[52] G. Ferrini, A. Minguzzi, and F. W. J. Hekking, Phys. Rev. A **80**, 043628 (2009).
[53] L. D'Alessio, Y. Kafri, A. Polkovnikov, and M. Rigol, Adv. Phys. **65**, 239 (2016).
[54] P. Scholl, M. Schuler, H. J. Williams, A. A. Eberharter, D. Barredo, K.-N. Schymik, V. Lienhard, L.-P. Henry, T. C. Lang, T. Lahaye *et al.*, Nature (London) **595**, 233 (2021).
[55] S. Ebadi, T. T. Wang, H. Levine, A. Keesling, G. Semeghini, A. Omran, D. Bluvstein, R. Samajdar, H. Pichler, W. W. Ho *et al.*, Nature (London) **595**, 227 (2021).
[56] T. Brydges, A. Elben, P. Jurcevic, B. Vermersch, C. Maier, B. P. Lanyon, P. Zoller, R. Blatt, and C. F. Roos, Science **364**, 260 (2019).
[57] T. L. Nguyen, J. M. Raimond, C. Sayrin, R. Cortiñas, T. Cantat-Moltrecht, F. Assemat, I. Dotsenko, S. Gleyzes, S. Haroche, G. Roux *et al.*, Phys. Rev. X **8**, 011032 (2018).
[58] T. Comparin, F. Mezzacapo, and T. Roscilde, Supporting data for "Multipartite entangled states in dipolar quantum simulators" (2022), 10.5281/zenodo.6534223.